Preprint typeset in JINST style - HYPER VERSION

Development of a Detection System to Measure Low Levels of ^{210}Pb using β/γ Coincidence

M. Widorski[a]*, E. Meehan[c], J. Monroe[a], A. Murphy[b], S. Paling[c], and D. Sanderson[d]

[a] *Royal Holloway University of London,*
Department of Physics, Egham Hill, Surrey TW20 0EX, UK
[b] *University of Edinburgh,*
Department of Physics, Address, Country
[c] *Boulby Underground Laboratory,*
Address, Country
[d] *University of Glasgow,*
SUERC, Address, Country
E-mail: markus.widorski@gmail.com

ABSTRACT: A new detection system was developed to measure activities of ^{210}Pb in the sub-mBq range in processed acrylic samples. The measurement method was based on the detection of coincident low energy β/γ emissions from ^{210}Pb using two high-purity n-type Germanium detectors and internal liquid scintillation counting. The detection system, including data acquisition, control and analysis software was designed, built, installed and operated at the STFC Boulby Underground Laboratory. The system was calibrated with a prepared ^{210}Pb standard source where an absolute detection efficiency of 0.395 ± 0.016 % was determined. The background measurements using a blank sample revealed a ^{210}Pb-equivalent activity of 365 ± 35 mBq. The increased level was likely due to cross contamination in the background sample as ^{234}Th was identified as one contaminant. The background value measured led to a detection limit of 140 mBq at 2σ for a measurement live time of 5.9 days. Although the targeted limit in the sub-mBq range was not reached, the potential of the method was demonstrated. Improvements to further reduce the detection limit are also outlined.

KEYWORDS: Keyword1; Keyword2; Keyword3.

*Corresponding author.

Contents

1. Introduction

There is interest in a number of areas of science in measuring the ^{210}Pb content of materials at the mBq/kg level and below. ^{210}Pb is an important tracer isotope used in geochronology; due to its half-life it covers periods of a hundred years for determining absolute ages of sediments [1]. ^{210}Pb analysis is important in radiation protection for work places where high levels of Radon prevail. Experiments searching for very rare signal processes, such as dark matter interactions with atomic nuclei or neutrino-less double beta decay, require suppression of background particle interactions to the level of 1 background event per tonne of detector mass per year of live time. To reach these stringent levels requires control of radioactive impurities in detector materials at the level of 0.01-0.1 mBq/kg for ^{238}U and ^{232}Th backgrounds, and 1 mBq/kg for ^{210}Pb.

This radiopurity limit for ^{210}Pb is below what currently can be achieved by the available standard measurement techniques. Hence, such low-background experiments require a new method providing a lower detection limit. The objective of this work was to develop and prototype a technique to reach detection limits for ^{210}Pb in the sub-mBq range. This work developed a measurement system based on coincidence logic to decrease the ^{210}Pb detection limit below the values attained by the established methods.

1.1 ^{210}Pb Backgrounds

A dominant background contribution from radioactive isotopes in low-background experiments is from the decay chains of primordial radionuclides which are present in the earth's crust. The ^{238}U decay chain figures among the most important sources due to the relatively high abundance of this isotope. With a half-life of 4.5 billion years, many of the daughter nuclides are usually in a secular equilibrium with the U, depending on the supporting medium. Separation can occur at various places in the chain, like for ^{230}Th and ^{226}Ra, due to varying chemical behaviour and solubility [2].

The decay of ^{226}Ra produces the very mobile noble gas ^{222}Rn with a half-life of 3.8 days, which is sufficiently long-lived to escape easily from its production location. Radon can be implanted into surfaces because of its recoil kinetic energy after the decay from Radium, or, as in the case of acrylic, also migrate by gaseous diffusion. The diffusion length in acrylic e.g. is 0.11 mm, hence the daughter nuclides can be deposited into depths of 1mm [3]. ^{222}Rn decays through a number of short-lived isotopes into ^{210}Pb, which has a half-life of 22.3 years. The activity of ^{210}Pb is not necessarily related to the current ^{222}Rn activity as the latter can change in concentration quickly depending on the environmental conditions while the lead is built up. ^{210}Pb forms a sub-series, and decays via ^{210}Bi (5 days) and ^{210}Po (138.3 days) into the stable ^{206}Pb. In case no physicochemical separation occurs, the two daughters will reach a secular equilibrium with the ^{210}Pb activity after sufficient time.

In the ^{210}Pb sub-series, ^{210}Pb disintegrates by β decay with a Q-value of 63.5 keV, emitting β particles with maximum energies of 17.0 keV (84%) or 63.5 keV (16%). The mean energy per disintegration is 6.18 keV [4]. The first decay branch to an excited state of ^{210}Bi is followed by a γ emission which competes with an internal conversion process. The total internal conversion coefficient α is 18.7 [5], resulting in an emission probability of only 4.25% for the 46.5 keV γ. The emission of the γ follows with a half life of less than 3 ns after the β decay.

1.2 Detection methods for ^{210}Pb

For the long-lived Uranium and Thorium isotopes, mass spectrometry offers the best detection limits [6]. Multi Collector - Inductively Coupled Plasma - Mass Spectrometry (MC-ICP-MS) is an established method to determine quantities of Uranium and Thorium in the ppt range [7]. However, since ^{210}Pb is a relatively short-lived isotope its detection and quantification is best done by radiometric methods. The most common are γ and α spectroscopy or β counting [6], which typically involve sample masses of a few grams.

γ spectroscopy relies on direct detection of the 46.5 keV γ using a low-energy sensitive semiconductor detector. Reverse electrode n-type HPGe detectors with thin windows made of Beryllium or Carbon are the state-of-the-art detectors used for this purpose. Typical detection limits in literature for direct γ detection are on the order of hundreds of mBq. Two references give detection limits of 440 mBq (sediments) [8] or 172 mBq (lead) [9].

α spectrometry is used to determine the ^{210}Po activity. This requires the application of radiochemical procedures before electro-depositing either the ^{210}Pb or ^{210}Po into a very thin layer on a metal disk to minimise self absorption in the sample. For both isotopes, spontaneous deposition is possible onto Ni or Ag in some cases without applying complex radiochemical methods. Some aspects and difficulties of ^{210}Po analysis are discussed in [10]. In general, when applying radiochemical methods, a tracer nuclide is required to determine the chemical yield of the procedure. Care must be taken that the ^{210}Po is in equilibrium with the ^{210}Pb, or that the exact separation and build-up time is known, when applying this indirect activity measurement of ^{210}Pb. Depending on the selected isotope and method, sufficient time must be allowed to grow in ^{210}Po before the measurement, this is typically several weeks or months due to the 138 day half-life of ^{210}Po. A semiconductor surface barrier or PIN diode detector is then used to detect the 5.4 MeV α particle from ^{210}Po. Alpha spectrometry currently offers the lowest backgrounds and a high detection efficiency. Typical detection limits for ^{210}Po by α spectrometry are on the order of 1 mBq [11, 8].

β counting or spectroscopy is used to measure the β particle of ^{210}Bi decaying to ^{210}Po. The endpoint energy of the β is 1.1 MeV (mean energy: 388.7 keV per disintegration), high enough to be easily detected with a proportional or other gas-based counter. Fairly complex sample preparation is usually required to remove interfering isotopes such as other beta emitters of naturally occurring isotopes and to transfer the sample into a thin layer to minimise self absorption. Liquid scintillation is also used to directly detect the low energy β from the ^{210}Pb decay. For the latter, radiochemical sample preparation is required and radioactive backgrounds in the sample, such as the build-up of ^{210}Bi, have to be considered in the analysis. Typical detection limits for ^{210}Pb by β counting of ^{210}Bi are 6 mBq [11] or 7 mBq [8] after radiochemical processing and measurement with a low background gas counter. A value of 33 mBq has been achieved for ^{210}Pb in liquid scintillation counting [6].

A new approach to detect low activities of ^{210}Pb based on coincident β/γ detection is developed in this work, combining liquid scintillation and gamma spectroscopy methods. The aim is to reach sub-mBq sensitivity, in an assay sample mass of order 1 kg.

2. γ/β Coincidence Counting

In the measurement method developed in this work, the β emission from ^{210}Pb is detected with

liquid scintillator in coincidence with signals from high-purity Germanium (HPGe) detectors to detect the 46.5 keV gamma from ^{210}Pb.

The coincident emissions from ^{210}Pb were already used in a different application for the precise determination of activities of radioactive standard sources [12]. As these measurements aim to determine absolute activities at high levels, detection limits are of less concern and were not stated. The classic coincidence method was applied by Woods [13], while a $4\pi\beta(LS)-\gamma(NaI)$ anti-coincidence method used at NIST [14] was first described by Baerg in 1981 [15].

The advantage of the coincidence technique is to greatly reduce random backgrounds. In the case of two channels in coincidence mode, an event must be detected in each channel within a time interval to be counted as a valid event. All events occurring alone in one or the other channel are rejected. This leads to a high rejection of random events, which are uncorrelated in time, while the system remains sensitive to time-correlated coincident events. However sources producing random events in both channels can still be detected in this configuration by simple chance. This chance coincidence rate r_{ch} from uncorrelated inputs is a function of the single input rates r_1,r_2 and the chosen coincidence resolving time τ [16]. 2τ is then the acceptance time window.

$$r_{ch} = 2\tau r_1 r_2 \tag{2.1}$$

The chance coincidence rate adds to the rate of true coincidences.

To obtain the efficiency of a coincidence counting system, the single efficiencies of the independent detectors multiply as only events generated by both systems at the same time are considered. As efficiencies are smaller than one, this effectively reduces the overall system counting efficiency. This is a disadvantage since it will increase the required counting time to achieve sufficient statistics. As long as the background rejection from the coincidences is large enough, the method remains advantageous. However, more stringent requirements ensue on system and sample stability and insensitivity to changes in the environmental conditions with longer counting times.

Using a coincidence method could potentially relax some requirements for specific low background materials for detectors, supports, shielding and the need to remove other isotopes from the sample to reduce some sample inherent background contribution. A direct measurement of the ^{210}Pb isotope will as well avoid the waiting time associated with grow-in of a daughter nuclide.

2.1 Liquid scintillation counting of the β emissions from ^{210}Pb

Liquid scintillation counting is a well established method to determine radioactivity in samples through detection of α or β radiation. The sample is mixed with or immersed into a scintillator cocktail to incorporate the decaying isotope inside the detecting medium. For many nuclides emitting low energy radiation, such as ^{3}H, ^{55}Fe or ^{32}P, liquid scintillation counting is the standard technique for environmental samples. ^{3}H, for example, emits a very low energy β particle (E_{max}=18 keV), which is easily detected by a liquid scintillator, but impossible to detect with any solid detector due to the self-absorption in the sample matrix. At this energy the range in e.g. silicon is on the order of 1 μm.

The liquid scintillator itself is the primary detector in this technique. The liquid scintillation cocktails commonly used consist of an organic solvent to which small amounts of scintillating components (fluors) are added [17]. The aromatic solvent makes up the major part of the solution

and absorbs the energy of the emitted radiation. A small part of the energy is transferred from the solvent to the scintillators. A primary scintillator emits light in the UV region below 400 nm, where photomultipliers initially were not very sensitive. Therefore a secondary scintillator is added to act as a wavelength shifter to move the light emission spectrum into regions of higher PMT sensitivity [17].

The number of photons emitted will be approximately proportional to the energy deposited by the radiation in the cocktail. This is roughly true for electron energies exceeding a certain initial energy. Below this energy, non-linearities can occur which are described by the empirical Birk's law. The liquid scintillator cocktail and sample mixture needs to be transparent to the emitted scintillation light to not quench the signal. Quenching is one of the major problems in liquid scintillation counting, as the sample matrix, the sample-cocktail-mixing-ratio and even the temperature can have a negative impact on the quenching behaviour. The scintillation light emitted by the detector is measured by photomultiplier tubes. Any quenching occurring in the detector volume or between the detector and the PMT shifts the measured energy spectrum to lower energies, and so effectively reduces the detection efficiency.

In order to detect the β in our γ/β measurement we use two photomultiplier tubes in a coincidence setup, in opposing positions with the scintillator sample matrix placed in-between. This reduces random backgrounds generated in the PMTs, while the system remains sensitive to light emitted from the scintillation detector volume. As the light is emitted isotropically from the detector, the coincident signals from both PMTs are summed and the detection efficiency is increased.

Typical internal backgrounds generated in liquid scintillation are the creation of light by chemical reactions (chemiluminescence) or delayed light emission after exposure to strong light sources (photoluminescence). The detector is sensitive not only to radiation emitted by nuclides contained in the sample or the cocktail, but as well to external sources. γ radiation, neutrons or muons can induce scintillation light emission which will be detected by the PMTs. Further, incident particle scattering can produce Compton electrons which may be in the energy range of the β particles of the isotopes under investigation. In general, the liquid scintillation counting chamber therefore is housed in a heavy shielding (lead, tungsten) to reduce the effect of external γ radiation, and special low radioactivity materials with reduced contents of Uranium, Thorium and ^{40}K are used for the photomultipliers, sample vials and cocktail components to reduce the γ induced background.

^{210}Pb measured in liquid scintillation will produce a complex energy spectrum due to multiple decays originating from the three isotopes ^{210}Pb, ^{210}Bi and ^{210}Po. Figure 1 shows such a composite spectrum [12].

2.2 HPGe counting of the γ emission from ^{210}Pb

For γ spectroscopy HPGe detectors offer unrivalled energy resolution at high efficiency with large volume crystals. In these detectors, a reverse bias is applied onto a diode.

For low-energy γs, a thin detector entrance window is required to minimise the absorption. Typical window thicknesses of Beryllium or Carbon are on the order of 0.5 mm [18]. Both elements have a small Z value, hence offer a relatively small absorption of low energy photons. Low energy sensitive detectors are operated in reverse mode (n-type crystal), having the p-type contact facing towards the sample. The p-type contact is typically produced by ion-implanted boron, giving the lowest possible dead layer thickness of less than a micrometer [18].

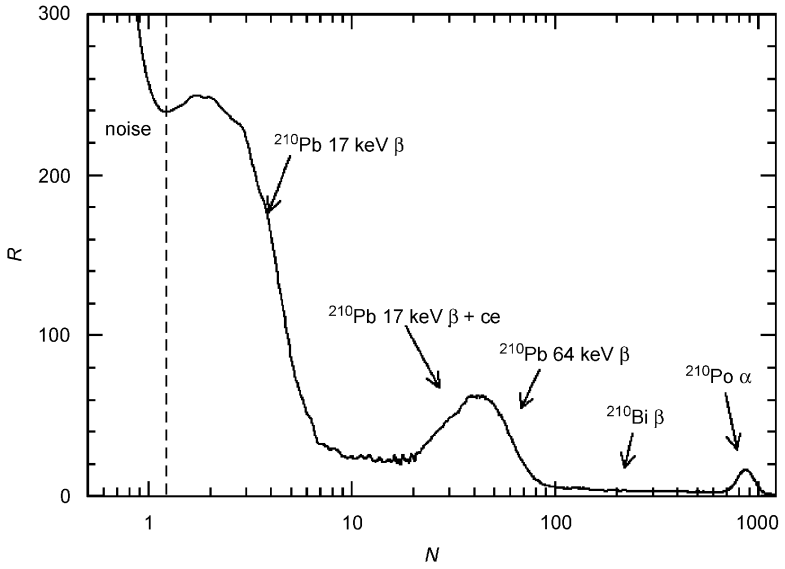

Figure 1. A typical liquid scintillation spectrum of ^{210}Pb, containing ^{210}Bi and ^{210}Po. The spectrum is assembled using three measurements at different gains to cover the large range. N is the channel number, R is a normalised gross rate. Taken from [12].

Detectors can be built of low background housing material, although this is not standard for commonly sold devices. For ultra-low level activity measurements, detectors are typically installed underground where the influence from and activation of the detector material and crystal is reduced, due to a low cosmogenic particle flux.

3. Experimental Setup

The schematic of the experimental apparatus built to test the coincidence method of ^{210}Pb measurement is shown in Figure 2 (not to scale). The sample is enclosed by two high-purity Germanium detectors (HPGe) facing each other to increase the overall geometric efficiency. Perpendicular to the HPGe axis, an acrylic sample holder and light guide fills the gap between the HPGes. The liquid scintillator generates light from the energy deposition of the beta particle in in the sample volume. The UV/visible photons are transported along the light guide and detected by two attached photomultiplier tubes (PMTs). The light guide is wrapped in diffuse reflecting PTFE to increase the light yield on the PMT photocathodes by internal reflection. The coincident gamma can be detected by one of the HPGe detectors.

To take advantage of the background rejection offered by the coincidence technique, both detection systems should feature a reasonably low background, high energy resolution and fast signals. A high resolution is advantageous to minimise the respective energy windows so to reduce the individual background count rates. Fast signals will allow shortening the resolving time in the coincidence logic and hence directly improve the rejection of random background signals.

Remaining background sources, which could possibly produce a valid signal after the coincidence discrimination, can be classified as follows:

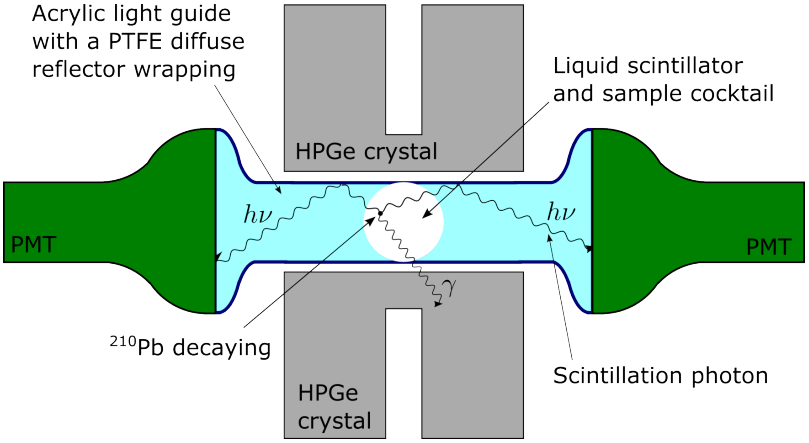

Figure 2. Schematic (not to scale) of the beta/gamma coincidence detection principle applied in this setup. A decaying ^{210}Pb nucleus embedded in the liquid scintillator emits a beta and gamma particle. The beta has only a short range of a few μm and generates scintillation photons by interacting with the liquid scintillator cocktail. The photons, emitted isotropically are detected by the PMTs. Simultaneously, the emitted gamma can be detected in one of the two HPGe detectors.

- any ^{210}Pb content in the materials in close contact with or dissolved in the liquid scintillation detector. This includes the inner surfaces of the sample volume, the liquid scintillator cocktail itself and any added solutions. Exposure to Radon or Radon progenies during the sample production could be problematic as well.
- any isotope undergoing a decay in the sample volume with coincident beta/gamma, where the gamma energy can scatter down into the relevant range with an associated beta particle in the low energy range.
- photons from external and internal sources undergoing Compton scattering in the liquid scintillator volume, where the scattered photon is detected by one of the HPGe detectors in the relevant energy range while simultaneously the photons produced by the Compton electron are detected in the PMTs.
- any events occurring at the same time by chance in the relevant energy ranges in the HPGe and PMT detectors.

To provide passive shielding, the setup was installed underground at the STFC Boulby Underground Laboratory [19] below 2805±45 m w.e. overburden [20], enclosed in a specifically designed low background lead and copper castle. Approximately 2 tons of lead and 270 kg of copper were used to shield the sample and detectors against external gamma radiation. The shielding thickness was at least 5 cm of copper and 15 cm of lead surrounding the sample in all directions. Figure 3 shows the uncovered detectors.

3.1 Estimated Sensitivity

A rough estimation of the potential performance was made before prototyping. The efficiency estimated from geometrical considerations for the double gamma detectors separated by 4 cm with

crystals of 5.5 cm diameter is 39%. The average self attenuation in the sample and sample holder is approximately 30% over 1.5 cm, estimated from the values for 47 keV photons in water [21], which has a roughly similar density to liquid scintillator [22]. With full absorption in the detector, this would lead to a total gamma detection efficiency of about 28%. The detection efficiency estimate for the liquid scintillation counting was based on values given for ^{3}H in literature for commercial devices. Typical values are on the order of 30% [23]. Considering the gamma emission probability I_γ, the branching ratio for the 17 keV beta B_β and the detection efficiencies ε_γ and ε_β, the overall efficiency ε_{total} is calculated as:

$$\varepsilon_{total} = \varepsilon_\gamma \cdot I_\gamma \cdot \varepsilon_\beta \cdot B_\beta = 0.28 \cdot 0.0425 \cdot 0.3 \cdot 0.84 = 0.3\% \tag{3.1}$$

For a sample containing 1 mBq of ^{210}Pb this would result in a count rate of 0.259 counts per day (=$3\cdot10^{-6}$ cps). This very low count rate requires measurement times of several days or weeks to obtain sufficient statistics, and therefore system stability is of high importance.

To estimate the potential chance coincidence background, values were taken from literature. The lowest value found for a background count rate of a sandwich HPGe detector, at the 46.5 keV peak, was $2.3\cdot10^{-5}$ cps (2 cpd) [24]. This was measured by an ultra-low background system. A more comparable value to our HPGe standard detectors of $1.5\cdot10^{-3}$ cps/keV in the 46.5 keV region [25], in an energy window of 2 to 4 keV, was reported from a semi-planar low-energy HPGe detector recently installed at the STFC Boulby Underground lab. For a liquid scintillation counter, we found typical background count rates for a commercial counter measuring ^{3}H [23], with a similar energy range as for ^{210}Pb, of 0.067 cps for a sample of low-background Ultima Gold LLT scintillator [23]. This is a very optimistic value considering that commercial devices have been optimised over many years, integrating methods to actively discriminate background events. A conservative estimate could be a factor 10-100 higher, for the purpose of this study we assume 6 cps. As an optimistic assumption a coincidence window of 50 ns would cover the events registered by the PMT and HPGe detectors emitted from a ^{210}Pb decay. The actual time window depends on the scintillator time constant, the precision of the pulse time measurement and the trigger arrangement. The chance coincidence background rate, from equation 2.1, is then

$$r_{ch} = 50 \cdot 10^{-9} s \cdot 0.0015 s^{-1} keV^{-1} \cdot 4\ keV \cdot 6 s^{-1} = 1.8 \cdot 10^{-9} s^{-1} = 1.55 \times 10^{-4} d^{-1} \tag{3.2}$$

Compared to the expected count rate of 0.259 cpd for a 1 mBq source, this chance coincidence background is negligibly small. With a potential S/N ratio of 1500, some margin is left for imperfections in efficiency or the assumed background parameters. However this chance rate does not include any background coming from impurities in the sample or the sources discussed in Section 3. These internal backgrounds will certainly be the limiting factor for the achievable detection limit. For this reason, we also made a control measurement of a blank sample which undergoes the same processing steps as the real sample.

3.2 Beta detection system

The β detection system consisted of two PMTs viewing the sample-loaded scintillator vial through an acrylic light guide.

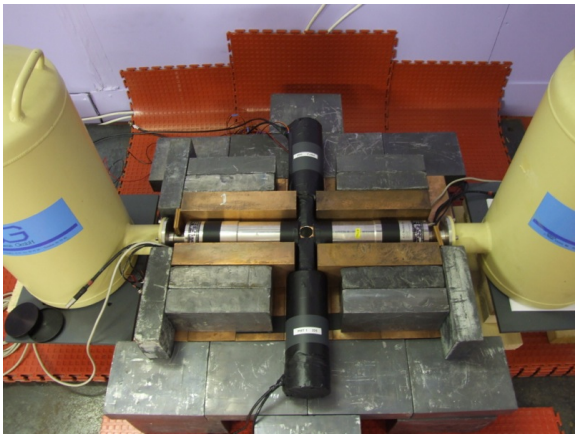

Figure 3. Complete setup with two HPGe detectors, the sample holder and light guide with attached PMTs on the shielding base plate. This setup was further covered with a layer of Cu bars and lead bricks.

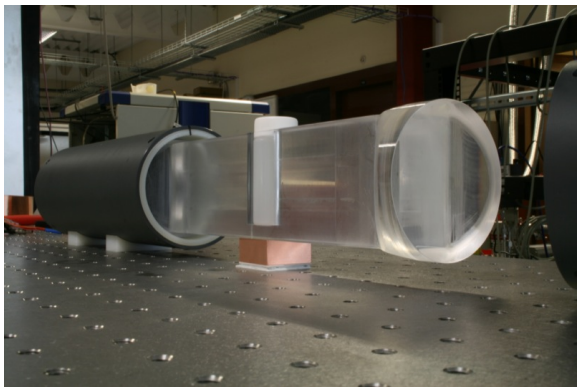

Figure 4. Acrylic light guide sitting on a Cu cold finger and incorporating a sample vial. In the back, a grey tube to house one PMT is attached. In the front, the polished circular face to couple a PMT is visible.

3.2.1 Sample holder

To contain the liquid scintillator and the sample solution an industrial standard laboratory vial was used. The container is a 20 ml vial, of 27 mm diameter and 61 mm height. The walls have a uniform thickness of 1 mm. The diffuse, but highly transparent to UV, polyethylene vial material is PTFE coated on the inside to prevent diffusion of solvents through the vial. The coating thickness is a few micrometers only, hence does not degrade the light transmission. These vials have been developed especially for use with liquid scintillation cocktails, where care is taken for low activity content and contamination free material [26].

To optimise light transmission from the sample to the photomultiplier tubes, the vial was placed inside an acrylic light guide with a refractive index of n=1.49 [27]. The light guide shown in Figure 4 was machined out of a cylindrical piece and polished on the front faces. Good optical matching was obtained by coupling the sample vial optically with silicone oil (n=1.44) to the sample holder. The PMTs were coupled to the polished circular surfaces of the light guide using an optical coupling grease (JRM: INCLUDE PRODUCT NAME). The light guide was wrapped in three layers of PTFE tape of 0.2 to 0.6 mm thickness to improve the indirect light transmission from the sample to the PMTs by adding diffuse reflection at the acrylic surfaces. The whole assembly was enclosed by aluminium foil and copper tape and sealed light tight with black tape. The only parts left uncovered were two circular areas facing the HPGe detectors and the top opening to insert and remove the sample vial.

3.2.2 Liquid scintillator

This application is fairly similar to ^{3}H counting, and so scintillator cocktails optimised for ^{3}H detection should be suitable. Such cocktails typically feature low chemiluminescence and reduced background in the low energy region. Based on the literature [28, 29, 30, 31] and the technical documentation of the manufacturer [23], the Ultima Gold uLLT cocktail was selected. Ultima

Gold uLLT is a comparable version of Ultima Gold LLT where the ^{40}K content is reduced by raw material selection [23].

Temperature affects the sample load capacity as well as the longterm stability and chemiluminescence. Depending on the nature of the sample solution and load, the mixture will show increased quenching due to greater opacity or inhomogeneities from phase separation at increased temperatures. In [28] the impact of the temperature on the scintillation cocktail and sample was investigated. Based on this work, and on our own visual observation of a marked difference in sample transparency at 22 deg C vs. 8 deg C, we cooled the sample during the measurement. The aim of the cooling system was to keep the sample in the temperature range of 10-15 deg C, which given the chosen sample load should keep the cocktail/sample mixture stable.

The cold side of a Peltier cooling element with 35 W cooling power and a surface area of 3cm x 3 cm was thermally coupled via a Cu block to the acrylic sample holder, just underneath the sample. The hot side was coupled to the copper shielding surrounding the whole setup. The 270 kg of copper and approximately 2 tons of lead serve as a heat sink further dissipating the total thermal power of 60 Watt to the environment via convection and thermal radiation. A further external cooling system, blowing air of 10-15 deg C inside the shielding on top of the sample at a few litres per minute, helped to reduce the temperature.

Acrylic is a very good insulator and poor heat conductor and therefore not an ideal material for cooling the sample inside. The light guide was therefore insulated itself as well as possible to reduce the heat transfer from the surrounding material through radiation and convection. The acrylic was wrapped in several layers of aluminised mylar to reflect heat radiation and reduce air convection. Several parts of the sample holder surface could not be insulated, such as the PMT connection faces, the sample loading opening on the top, the side faces towards the HPGe detector windows and the bottom where the cooling contact was made. Additional plastic foam parts were placed along the light guide to insulate towards the top and bottom copper bars.

After a few hours of operation, the temperatures measured at the bottom of the sample hole were approximately 8 deg C and stable. However, the gradient towards the top of the sample was substantial, reaching up to 17-18 deg C at a room temperature of about 24 deg C. Likely the heat conduction through the entire copper shielding was not good enough, because of poor coupling between the individual copper bars. We proceeded with this cooling setup for the prototype test because the samples showed no clouding effect after several days in the sample holder. However a weak inhomogeneity in density was observed from the bottom to the top for the blank sample and calibration source.

3.2.3 Photomultiplier tubes (PMT)

The photomultipliers in this experiment had been previously used for the ZEPLIN-III anti-coincidence veto detector [32]. The model ETEL 9302KB PMTs are 3" circular flat-surface tubes with a bi-alkali high efficiency photocathode [33]. They are operated at negative bias with a direct coupled fast signal output from nine amplification stages. The PMTs were selected for their low intrinsic background level and had been screened before the use on the ZEPLIN-III detector [32]. Contents of Uranium, Thorium and Potassium were specified by the manufacturer at levels of 30 ppb, 30 ppb and 60 ppm. The PMTs were used with their fitted voltage divider networks (ETL C647BFN2-01) and operated at voltages -1070V and -1150 V. The timing properties according the technical data

Table 1. PMT parameters as determined by the ZEPLIN-III collaboration [34].

PMT S/N	225	1059
Quantum efficiency @420nm	28.43	29.55
Voltage @ 50A/lm [V]	-925	-819
Voltage @ 200A/lm [V]	-1124	-992
D/C @ 50A/lm [nA]	0.430	0.496

Table 2. Results from dark runs to determine the single photoelectron peak position.

PMT	HV [V]	Threshold [mV]	Count rate [cps]	SPE peak [mV]
PMT1 (225)	1150	11	9654	27.7 ± 0.9
PMT2 (1059)	1070	11	9866	34.5 ± 0.3

sheet [33] were 40 ns transit time, and the multi electron rise time and FWHM were s7.5 and 15 ns, respectively.

For ZEPLIN-III, the PMT was fitted with a simple preamplifier stage with a gain of $\sim$10, shaping the signal to a 40 ns rise time and 3 μs fall time. The preamplifier allowed impedance matching with their digitiser system and moreover to better cope with their maximum possible sampling rate of 100 MHz. In this setup the preamplifier was removed. This decision was motivated by an observed saturation of the preamplifier signal at 240 mV, corresponding to approximately 5-6 detected p.e.. A further reason was the requirement to obtain a precise measurement of the photon arrival time and separation between pulses. Without preamplifier, the typical pulse width measured was about 25 ns. The signal however, needed to be amplified by an analogue fast amplifier with a gain of 10 to obtain a large enough signal.

To determine the single photoelectron (SPE) amplitude, runs were performed for each PMT in the final setup, at stabilised temperatures, after one day operation at HV in darkness, without any scintillator sample or light source present. The dark count rate from thermo-ionic emissions at approximately 0.3 p.e. was rather high at around 10,000 cps for each PMT. The PMT signals were triggered by an external discriminator module set at 11 mV threshold ($\sim$ 0.3 p.e.) above baseline. In the data analysis later the same threshold was used. The amplitude spectra were fitted with a gaussian function to obtain the position of the single photoelectron peak. This is a simplified approach as it does not precisely model the underlying p.e. amplitude distribution. The resulting SPE peaks were at 27.7 and 34.5 mV, with a variation of 3% and 1% after cycling the HV. Table 2 lists the measured values.

3.3 Gamma detection system

For the gamma detection, two high-purity Germanium detectors of type NGC-3020, S/N GI-722 (D1) and GI-723 (D2), from DSG Detector Systems GmbH were used. The detectors were equipped with coaxial n-type crystals of 55.7 mm diameter and 57 mm length with a relative efficiency of 30%. The crystal was placed under vacuum approximately 5 mm behind a Beryllium window of 0.5 mm thickness. Each detector was cooled by a 15 litre LN_2 dewar. Both detectors

Table 3. Results of background and screening runs made with the two HPGe detectors GI-722 (D1) and GI-723 (D2), placed inside and outside the Cu/Pb shielding. With D1, two additional runs were made to screen a bottle with 0.5l of Ultima Gold AB scintillator and one PMT ETEL 9302KB.

Detector	Run	Count rate in interval		Meas. time	Comment
		44-48 keV	40-3000 keV		
		[cps/keV]	[cps/keV]	[h]	
D1	11-12	0.0260 ± 0.0012	11.51 ± 0.06	55	unshielded
D1	11-27	0.0316 ± 0.0012	12.08 ± 0.07	24	unshielded
D1	12-28	0.0021 ± 0.0004	0.49 ± 0.01	131	shielded
D1	12-10..13	0.0027 ± 0.0005	0.50 ± 0.01	66	shielded + LS
D1	12-13..25	0.0022 ± 0.0004	0.50 ± 0.01	119	shielded + PMT
D2	12-10	0.0573 ± 0.0018	18.70 ± 0.09	120	unshielded
D2	12-28	0.0575 ± 0.0019	18.45 ± 0.08	131	unshielded
D2	11-12	0.0049 ± 0.0006	0.56 ± 0.01	56	shielded
D2	11-27	0.0051 ± 0.0006	0.55 ± 0.01	41	shielded

featured an integrated resistive feedback preamplifier, providing two signal outputs and one test input connection. Detector 1 was operated at a negative bias of -3000V, detector 2 at -2500V.

3.3.1 Background level

To determine the background level with and without Cu/Pb shielding and to screen a flask of Ultima Gold AB liquid scintillator and one PMT ETEL9302KB, a number of runs were performed, listed in Table 3. The detectors were installed at the STFC Boulby Underground Laboratory and tested over a period of two months inside and outside a shielding of 5+15 cm of copper and lead. The performance of the Germanium detectors was checked using a standard analog amplification chain with shaping amplifiers (gain 50, shaping time 6 μs) and 8k multi channel analysers.

In both detectors, the background runs revealed the presence of ^{210}Pb by a prominent 46.5 keV peak giving the count rates shown in Table 3.4, most likely from contamination on the detector entrance windows. Detector 2 shows about a factor 2 higher count rate in the region 44 to 48 keV compared to Detector 1. It is suspected that this contamination originates from long-term Radon exposures to the surface air, as both detectors had been built almost 19 years ago and stored in surface laboratories since.

3.3.2 Energy calibration

The energy calibration of the detectors was done using ^{210}Pb, ^{57}Co and ^{60}Co standard radioactive sources. The energy stability was verified at least once and further checked using U/Th chain peaks in the background spectra. No significant energy shift was observed during the operation period.

The detection efficiency relative to a 3"x3" NaI detector was verified for both detectors. A ^{60}Co point source of known activity was placed at 25 cm distance of each detector. The obtained absolute net peak efficiency was then normalised with the NaI absolute peak efficiency of $1.2{\cdot}10^{-3}$ [16, p.459] to determine the relative efficiency. The specified values of about 30% were both confirmed closely to 31.5% and 32.2% for detector 1 and 2, respectively (Table 4).

Table 4. Resolution performance of HPGe detectors GI-722 (D1) and GI-723 (D2) as specified by the manufacturer and confirmed in measurement with calibration sources ^{210}Pb (Env. sample), ^{57}Co (B030) and ^{60}Co (B016). Given are the FHWM in keV and the relative resolution measured with a shaping time of 6 μs.

Detector	Serial	Rel. Efficiency	Energy	Specified resolution		Measured resolution	
			[keV]	[keV]	[%]	[keV]	[%]
D1	GI-722	30.2% (spec.)	46.5			1.31	2.8
		31.6% (meas.)	122	0.84	0.7	1.23	1.0
			136			1.26	0.9
			1173			1.94	0.17
			1332	1.87	0.14	2.08	0.16
D2	GI-723	30.5% (spec.)	46.5			1.30	2.8
		32.2% (meas.)	122	0.86	0.7	1.20	1.0
			136			1.22	0.9
			1173			1.78	0.15
			1332	1.81	0.14	1.80	0.14

The resolution performances as specified by the manufacturer were checked by measurement with ^{210}Pb, ^{57}Co and ^{60}Co calibration sources. The results are given in Table 4. As shown, the specified resolutions could be reproduced at high energies, while at low energies, the resolution increased above the specified values, likely due to the relatively larger contribution of electronic noise. In the final measurement configuration, high and low frequency noise modulated between V_{pp}=1 to 4 mV.

For the β/γ coincidence measurement, a remote-controllable, oscilloscope was used for the data acquisition system (DAQ) was used. For this, the analogue amplification chain and MCA were replaced and the HPGe preamplifier outputs were input to the digital oscilloscope. No additional analogue amplification of the HPGe preamplifier signals was made.

In this configuration, the preamplifier output pulses were checked for their rise and fall times. The signal rise time (10-90%) was measured to approximately 180±30 ns on both detectors, while the fall time (90-10%) was approximately 100±20 μs. The oscilloscope provided only a 8 bit resolution for the amplitude measurement, limiting the energy resolution and actual usable voltage range. For the low energies of ^{210}Pb and ^{57}Co, the smallest possible scaling division of 2 mV/div was selected, giving a full scale of 16 mV. For the ^{137}Cs source, a 10 mV/div scaling was required. With these settings, waveforms were acquired and processed offline to generate pulse height spectra. A linear energy calibration using the ^{57}Co and ^{137}Cs peaks was taken to the determine the expected 46.5 keV peak position. The calibration factors were fitted to 15.46 keV/mV and 16.07 keV/mV for detector 1 and 2, respectively. For both detectors, the predicted and measured position (using ^{210}Pb-loaded calibration scintillator sample, described in the next section) matched. The calibration ^{210}Pb spectra are shown in Figures 12 and 13. The peaks were fitted with gaussian functions to determine peak position and peak width. The resolution found for the peaks in the digital setup were about a factor 4 to 10 worse compared with the values found in the analogue setup. The reason for the resolution degradation in the digital setup was not found, and in future work the digital acquisition system will be upgraded.

Given the energy calibration, the integral between 2 mV and 3.2 mV would correspond to 30.9 keV to 49.5 keV for Detector 1 and 32.1 keV to 51.4 keV for Detector 2. From the simulated spectrum, taking into account this large part of the Compton continuum, which is signal induced, gives an increased efficiency of 39.7% compared to 26% only for the full energy peak.

3.4 Calibration and Assay Samples

Three scintillator samples for the calibration, background and acrylic assay measurement were prepared in a Clean Room class 10,000, to avoid contamination of samples by Radon progenies. The calibration sample was used to determine the detection efficiency of the γ/β coincidence method, and the background sample was used to set a sensitivity limit to ^{210}Pb. The acrylic assay measurement sample has not yet been measured, however the preparation is described here because it motivated a number of the experimental choices for the coincidence tecnique. The sample properties are summarized in table 6.

3.4.1 Acrylic sample

This measurement was specifically motivated by the need to screen acrylic material for ^{210}Pb content for dark matter searches. Common to all potential detection methods for ^{210}Pb in acrylic is the requirement to reduce the volume of the acrylic in order to make the low content of ^{210}Pb and its progeny accessible to detection. A procedure to break up the acrylic matrix had been already developed for the SNO experiment [35] and taken up again by DEAP. A team at Queen's University in Kingston, Canada, is currently working on the physicochemical procedure to vaporise and incinerate the acrylic while keeping ^{210}Pb and other heavy isotopes with a high boiling point in the solid remainder. Their further objective is then to measure the residuals by gamma and alpha spectroscopy [36].

The procedure under development at SNOLAB is described briefly in the following. Polymethyl methacrylate (PMMA, acrylic) consists of polymerised $(C_5O_2H_8)_n$. The PMMA samples are heated to about 400degC in a nitrogen atmosphere, where MMA vapour is produced and transferred further to be incinerated at above 800degC [37]. It is expected that impurities such as ^{210}Pb will remain in the solid fraction, while other volatile components like ^{210}Po are removed with the gaseous phase [10]. The solid fraction is extracted using aqua regia, which is a mixture of HCl and HNO_3. The evaporation container is rinsed several times with aqua regia and ultra pure water to remove all residuals. The obtained solution then is further reduced in volume by evaporation. Effective overall volume reduction factors of 10^3 to 10^4 should be achieved with this method.

The final processing procedure as well as the required method to determine the chemical yield of the reduction process are still under development. As this method aims to process ultra-low concentrations of isotopes, great attention must be paid to the adsorption and chemisorption processes not to lose the small amounts of isotopes to be measured. Carrier addition, pH control and only wet process steps are key factors to obtain reproducible results and high concentration yields [38].

In order to test the compatibility of a sample solution from acrylic residues and the liquid scintillator, the vaporised sample ID 25 processed by the SNOLAB team on 29/08/2012 was used. 619g of acrylic were vaporised and incinerated. The residues were extracted by 2 x 50ml of aqua regia and 20 ml of ultra pure water. The total volume of 120 ml was further reduced by evaporation down to about 2 ml. This processing was performed at SNOLAB. At RHUL, the 2 g 'acrylic' acid

Table 5. Calibration sources used in this experiment.

Nuclide	Half life [d]	Activity [kBq]	Unc. [kBq]	Ref. date	Activity (1/4/13) [kBq]	Unc. [kBq]	Identifier
^{57}Co	271.8	370	18.5	12/12/05	0.411	0.021	B030
^{60}Co	1925	37	1.9	01/12/00	7.31	0.37	B016
^{60}Co	1925	14.9	0.7	14/11/12	14.2	0.7	B032 (NW111)
^{137}Cs	10983	444.1	22.2	07/05/13	445.1	22.3	PX947
^{137}Cs	10983	4.5	0.2	07/05/13	4.5	0.2	RN290
^{210}Pb	8145	unknown					Env. sample
^{210}Pb	8145	0.523	0.006	04/12/12	0.518	0.006	in LS

solution was transferred into a 20 ml sample vial. The sample bottle was rinsed once using approx. 3 g of 0.1 M HNO_3. Then approximately 15 g of liquid scintillation cocktail Ultima Gold uLLT was added and the vial closed. The exact quantities are given in Table 6.

3.4.2 Calibration sources

A small amount of a liquid ^{210}Pb calibration standard was obtained from the SUERC Glasgow. The standard solution had an initial activity of 1072.8±12.4 Bq/g ^{210}Pb on 22/4/1993. 1.0825 g of this 2 M HNO_3 was diluted by 4.0887 g H_2O to obtain a total mass of 6.0712 g of 0.4 M HNO_3 containing 629±7 Bq on 4/12/2012. The uncertainty of the activity is governed by the uncertainty of the primary standard, not by the uncertainty of the weighing procedure, which was in the 0.1 g range. Approximately 5 g of this solution were mixed with 15 g of liquid scintillator in a vial. The exact amounts are given in Table 6. The total contained activity of ^{210}Pb in the calibration vial was calculated to be 518±6 Bq on 1/4/2013. In addition to the produced ^{210}Pb source, a number of gamma emitter sources have been used for calibration. The complete list of sources used is given in Table 5. In particular, ^{137}Cs source data was used to verify that the scintillator quenching is the same between the calibration and background samples.

3.4.3 Background sample

To account for impurities contained in the liquid scintillator cocktail and the acid solutions or possibly introduced during the preparation process, a blank sample was also prepared. Approximately 5 g of 0.1 M HNO_3 was mixed with 15 g of liquid scintillator. The 1 M HNO_3 had been prepared at SNOLAB under the same conditions as all other sample processing steps and using the same lot of primary solution.

3.5 Data acquisition and control system

The data acquisition and control system comprised the parts to control the detectors and auxiliary equipment, and to acquire, store and transfer data. It consisted of two NIM crates for analogue nuclear instrumentation modules, power supplies, a LabJack ADC/DAC interface, temperature probes, a digital oscilloscope, a computer and the corresponding software.

The central part of the DAQ was the digital oscilloscope performing the data acquisition. The device featured a PC operating on Windows XPe, which allowed to run automation scripts. A

Table 6. Samples and calibration source produced in the RHUL Clean Room. The uncertainty for each weight fraction is 0.1 mg.

	Weight [g]	Σ weight [g]
Background sample		
Vial	5.1724	5.1724
0.1 M HNO_3	5.0123	10.1847
Ultima Gold uLLT	15.5213	25.7060
net solution		20.5336
Acrylic sample (Vap ID 25)		
Vial	5.1018	5.1018
Sample VapID25	2.1162	7.2180
0.1 M HNO_3	2.9445	10.1625
Ultima Gold uLLT	15.6951	25.8576
net solution		20.7357
Calibration source		
Vial	5.1718	5.1718
^{210}Pb solution	5.0516	10.2234
Ultima Gold uLLT	15.6841	25.9075
net solution		20.7357

number of such Python scripts were developed controlling the various input and outputs as well as the data acquisition runs, file processing, backup and transfer. The external trigger signal was produced by analogue equipment. This was mainly motivated by the limited recording speed of the oscilloscope when acquiring waveforms and the requirement to determine the actual dead time of the system. The analogue nuclear instrumentation for each detector system was placed in a separate NIM crate to avoid cross talk issues.

As all equipment was installed underground at the STFC Boulby laboratory, most of the control functions were required to be remotely accessible. The oscilloscope and PC could be accessed remotely, to change settings, to start and stop runs, power the PMT HV and readout temperatures or to reboot the device. A separate remote power switch acting on both NIM crates was accessible via a dedicated phone line.

The control system included the HV modules for both HPGe detectors and PMTs, the power supply for the HPGe detectors, a ADC/DAC interface and a temperature monitoring probe. The LabJack U3-HV module is a USB powered ADC/DAC interface which allows to acquire or output a number of analogue low voltage signals. It includes amongst others a low power 5V supply and two channels which can be configured as digital counters. The high voltage supply for the HPGe detectors featured an automatic shutdown function based on a LN_2 level measurement system. The high voltage settings were -3000 V and -2500 V for detectors 1 and 2, respectively. The preamplifiers were powered using two NIM standard Timing Filter Amplifier modules ORTEC 474. These modules could not be controlled remotely. The high voltage to the PMT was supplied by a WENZEL N1130 module. The HV was set separately for each PMT and controlled remotely

via analogue low voltage signals produced by the LabJack. A LM335AZ-TO92 temperature probe was connected on top of the light guide close to the sample holder opening. The probe was powered and read out by the LabJack interface.

An additional computer, used for the initial test of the HPGe detectors, provided a visual control of the setup via a webcam to remotely verify the status of power supply, HV, LN_2 fill levels and the ambient temperature. It allowed as well to remotely switch the cooling system via a USB interface.

3.5.1 Trigger

The DAQ trigger was a logic OR between the HPGe signals. The single background rates of both HPGe detectors in the 44 to 48 keV window showed that one could expect trigger rates of less than 0.1 cps. Each HPGe detector provided two identical signal outputs, the second of which was amplified and fed into a single channel analyser (SCA) to produce a logic signal. Unfortunately only one Timing Filter Amplifier (TFA) channel was available, and so the signals of both detectors where added using a BNC T-type piece and fed into a single TFA. The signal, amplified by a gain of 250, was connected to the SCA, where a window was set to enclose the expected pulse height.

An approximate energy calibration of the amplified signal was made with sources using the oscilloscope to determine the upper and lower discrimination limits (LLD/ULD) of the SCA. The 662 keV peak was found at about 5.1 V, the 122/136 keV at 0.84/1.0 V and the 46.5 keV was expected at 0.36 V. With the ^{210}Pb source, the peak position could be confirmed at approximately 0.35 V for both detectors. The final window setting on the SCA was chosen to be 0.2 V (LLD) and 0.6 V (ULD) sufficiently covering pulses in the interesting energy range for both detectors. The lower level was set just above the baseline noise. Figure 5 shows an example screenshot of the persistent signals from HPGe detectors 1 and 2 using the ^{210}Pb source. The continuous baseline on both graphs come from a trigger on the respective other detector.

The SCA provided a fast NIM logic signal (20 ns) used to trigger the oscilloscope and a TTL logic signal (500 ns) connected to the LabJack counter. The signal was delayed by approximately 500 ns, hence a compensation offset of +500 ns was introduced to the oscilloscope timebase, centering the trigger signal.

The two counters of the LabJack interface were used to acquire the trigger signals in order to measure the data acquisition system deadtime. One channel was used for the trigger produced by the analogue discriminators. An auxiliary output from the oscilloscope was configured to output a logic pulse for each recorded event. This pulse was counted by the second channel. By acquiring the trigger externally, monitoring the progress of an ongoing run was possible without interfering with the file system or the data acquisition software.

3.5.2 Signal timing

The timing of signals between their generation in the detector and acquisition by the DAQ is of prime importance in a coincidence setup. Care was taken to use identical cables and cable lengths for the PMTs and the HPGe detectors respectively, to avoid tedious offline corrections. In order to check the actual time lag between the detectors, a pulser setup was used supplying synchronous test signals to all four detectors. The pulse generator triggered a blue LED with a 95 ns long square pulse, while sending another 1 ms long square pulse to the test input of both HPGe preamplifiers.

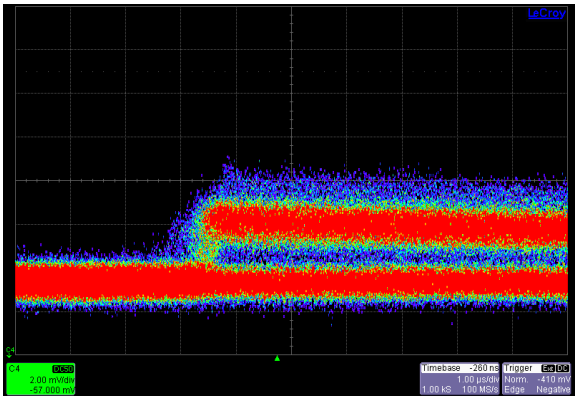

Figure 5. HPGe detector 1 preamplifier signal using a ^{210}Pb source, triggered by the HPGe based trigger setup. The difference between base line and signal is about 3 mV.

The LED was placed inside the sample holder. The LED pulse was delayed by 1ms in order to coincide with the falling edge of the HPGe test input pulse. There were two components where the introduced delays were not known: The preamplifier (denoted delay Y) and the LED (delay X), where a considerable delay between current rise and light emission was expected. These values were obtained from a specific pulser/LED run. Given the measured delays from each component, the PMT signals arrive at the oscilloscope with a delay of (56.4-Y) ns with respect to the HPGe signal. In the pulser/LED setup, the time difference is 44.4 +(X-Y) ns, due to the LED and additional delay of 12 ns for the test pulse towards the HPGe.

3.5.3 Digital Oscilloscope

The four input channels of the digital oscilloscope acquired the amplified PMT output pulses and HPGe detector preamplifier output signals, triggered by the external trigger circuit. All channels were set at 50 Ω input impedance. For the PMT this matched the output impedance of the Fan-in/Fan-out module and the cabling used. The output impedance of the HPGe detectors was 93 Ω, but the small mismatch did not manifest in visible reflection or signal distortions.

As all four channels used a common time base, a compromise setting needed to be determined. The PMT pulse width was approximately 25 ns for pulses in the few p.e. range, while the typical HPGe pulse rise time was on the order of 100 ns. For the HPGe pulses, sufficient time before and after the trigger was needed to reliably determine the baseline and the pulse height. Another constraint was the delay in the trigger pulse requiring an offset of +500 ns. A resolution in the nanosecond range was aimed at, while the number of data points per trace needed to be restricted, because this number directly affected the acquisition speed and the amount of data to be handled. A timebase setting of 200 ns/div was chosen, resulting in a total trace length of 2 μs. To obtain a sufficient time resolution of 2 ns, the number of samples was restricted to 1000 data points per waveform, equivalent to a sampling rate of 500 MS/sec. Typical recording rates at these settings for four channel were in the range of up to 10 Hz.

The voltage measurement delivers values over 8 divisions of a minimum scale of 2 mV/div at

a resolution of 8 bits (2^8-1 = 255 bins). The quantisation error for a 8-bit ADC is 0.113%. Unless otherwise noted, the minimum scale setting of 2 mV/div was used.

4. Results and discussion

In the following sections data sets from initial tests, calibration and background runs are analysed.

4.1 Data processing

The acquired waveforms were processed using a C++ library in ROOT [39], which was part of the software package developed for a Neutron Veto system at MIT [40]. The library was adapted to the specific needs of the actual setup, consisting of two PMT and two HPGe input channels. A Python script, included in the software package, called the library to batch process the waveform files and to transfer the raw data into a ROOT format file. At the same time some event processing was performed on the waveform data, such as peak identification and the determination of peak parameters like peak time, pulse start and end times, all stored along in the same ROOT file.

The baseline of a PMT signal was determined by evaluating the distribution of all voltage values in the waveform. The single peak found of this distribution was considered to be a good estimator for the baseline value since the possible bias induced by the presence of a peak in the waveform is negligible due to the narrow peak widths and small number of data points compared to the total trace length. The peak amplitude and time was determined from the maximum absolute voltage value of a peak found in the baseline-subtracted waveform.

For the HPGe signals, the histogram of waveform values resulted in a bimodal distribution, when the typical step-shaped pulse was present. The lower voltage peak was taken as the baseline value, while the higher voltage peak was considered for the pulse amplitude. With no clear step-shaped pulse, only a unimodal histogram was found, hence the waveform was considered to be pulse-free. The peak time was determined at the crossing of the 50% amplitude level.

4.2 Calibration runs

The analysis of the ^{210}Pb source runs performed to calibrate the detection system was done in three steps. Firstly, the stability of the data acquisition was checked. Secondly, a number of cuts were defined to clean the data in order to determine as a third step a value for the absolute detection efficiency based on the given source activity.

A total of 8 runs, adding up to 80,070 events, were made with the ^{210}Pb source and the HPGe trigger. The ratio between recorded and true trigger rate was 0.53, over a real time of 14,748 seconds ($\sim$ 4 hours). All DAQ settings remained unchanged over the runs.

To assess the detector stability, the recording data rate, baselines, amplitudes, peak times and peak time differences between PMT and HPGe, were plotted against the trigger time. All runs show stable pattern and average rates. As such all runs were considered for analysis with a constant dead time correction applied to the data set.

Table 7. List of data cuts applied on the calibration data set, and subsequently to the background data set. The upper and lower limits were derived from the data analysis of the calibration data set. The first three cuts and the PMT matched peaks cut was referred to as the 'basic cut'.

Cut	PMT1		PMT2		HPGe1		HPGe2	
	Lower	Upper	Lower	Upper	Lower	Upper	Lower	Upper
Peaks	-	-0.01	-	-0.01	peak found > 3 σ from baseline			
Boundary	0.3 p.e.	11.8 p.e.	0.3 p.e.	10.4 p.e.	-	-	-	-
Baseline	-0.023	-	-0.023	-	0.008	0.012	0.051	0.0535
Peak time	peak time in [800ns,1100ns]							
Matched$_{PMT}$	$\|\Delta t\|$ in [0ns, 40ns]							
Matched$_{PMTGe}$	$\|\Delta t\|$ in [0ns, 40ns]				Δt_{PMT-Ge} in [-250ns,0ns]			
Offset$_{PMT}$	$\|\Delta t\|$ in [460ns, 500ns]							
Offset$_{PMTGe}$	$\|\Delta t\|$ in [0ns, 40ns]				Δt_{PMT-Ge} in [250ns,500ns]			
Energy	[1 p.e., 5 p.e.] for PMT1+PMT2				2 mV	3.2 mV	2 mV	3.2 mV

4.2.1 Data cuts definition

A set of data quality cuts was defined to remove events that did not meet the criteria for valid events in terms of energy, coincidence time or timing interval. Table 7 summarises the cuts discussed in the following. The resulting survival fractions after the cuts are summarised in Table 8.

For all channels, events were removed where no peaks above the analysis threshold were found (peaks cut). 94% of all events had a HPGe peak, while a PMT peak was found in only 50% of the events.

Values falling outside the effective PMT measurement range, filling the overflow bin or populating the noise region at the lower boundary, were removed (boundary cut). This cut removed approximately 10% of the events for each channel. No boundary cut was needed for the HPGe signals, as the trigger already included this cut, by using an SCA window which was entirely contained in the measurement range.

Events with a baseline value 10σ away from he mean value were also removed (baseline cut). This cut aimed to remove waveforms where the baseline was obviously wrong and would bias the net amplitude. The event rejection was approximately 0.3%.

Events where HPGe peaks were not located in the defined trigger region between 800 and 1100 ns were removed (peak time cut). This cut removed 7.3% of all events. We assume that misplaced trigger signals are due to noise or off-scale signals and remove these events without correcting the live time.

Two cuts were applied on the coincidence timing. The $matched_{PMT}$ cut returned only PMT peaks which were coincident within the defined time window. This cut and all the aforementioned cuts are referred to as the 'basic cut' throughout this text. The $matched_{PMTGe}$ criteria was the coincidence between one of the HPGe peaks and matched PMT peaks.

The $matched_{PMT}$ cut was chosen based on the time difference between the PMT signals in the ^{210}Pb calibration data, shown in Figure 6. The cut window was set to cover the entire peak between -40 ns and +40 ns. 25.1% of events surviving these cuts.

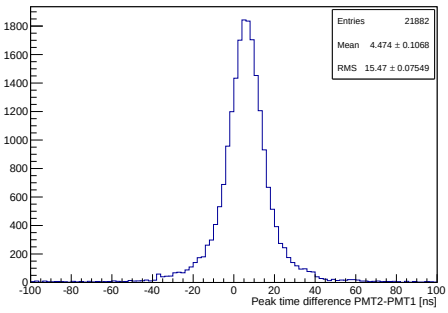

Figure 6. Peak time differences between both PMTs in the ^{210}Pb calibration data.

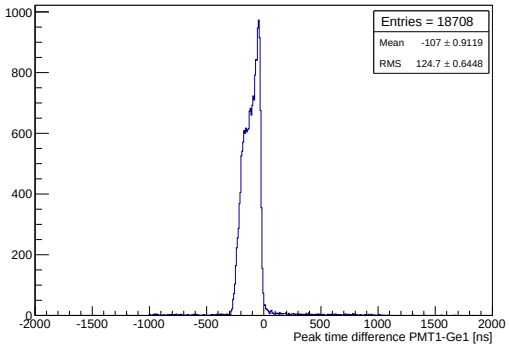

Figure 7. Peak time differences PMT1 - HPGe1 for events with peaks in the ^{210}Pb calibration data.

The $matched_{PMTGe}$ cut was chosen based on the peak time differences between PMT and HPGe signals with cuts for peaks, baselines and boundaries applied; an example is shown in Figure 7. A clear coincidence peak is visible between -250 ns and 0 ns. This peak is not located where assumed initially from the signal timing considerations and the pulser/LED tests. Here, the coincident signal peak would have been expected between 7 to 20 ns. The actual position was measured at -110±85 ns. It seems that the HPGe signal is delayed with respect to the PMT signals, and with a much larger time spread. The processing scripts had been verified that no bias was caused by an analysis artefact. Tests with the identically structured pulser/LED waveform data exclude this possibility. One explanation for the different location of the coincidence peak could be an additional delay in the charge collection from the Ge diode to the preamplifier. The spread in the time difference of 250 ns could be caused by an effect in the scintillator, such as delayed energy transfer from the solvent to the scintillator. Another factor adding a spread could be a time jitter on the HPGe peak times, which is expected to be larger for pulses close to the noise than for the large amplitudes created by the pulser. The cause of this timing discrepancy is currently not understood, and further investigations are required. To account for this uncertainty, the coincidence window was set to cover the entire region, [-250ns,0ns], for the time difference between PMT and HPGe signals.

The last cut applied limited the valid energy range to cover the approximate interval of the beta and gamma energies from ^{210}Pb (energy cut). The summed PMT signals vs. the HPGe amplitudes are shown in Figures 8 to 11, after the basic cuts for peaks, boundary, baseline, peak time and coincident peak matching between PMTs and PMTs and HPGe signals have been applied. The energy cut is set to cover the rather restrictive energy interval between 1 and 5 p.e. for the PMT sum, based on these figures, to reduce the influence from higher energy beta particles from other potential background sources. In order to cover the full peak in the HPGe detectors, the final energy cut window was set to include all pulses with amplitudes between 2 and 3.2 mV. However, this also includes part of the (signal induced) Compton continuum so also increases the measurement efficiency. In Figures 9 and 11 the energy cut for both the PMT sum and the Ge signals is also

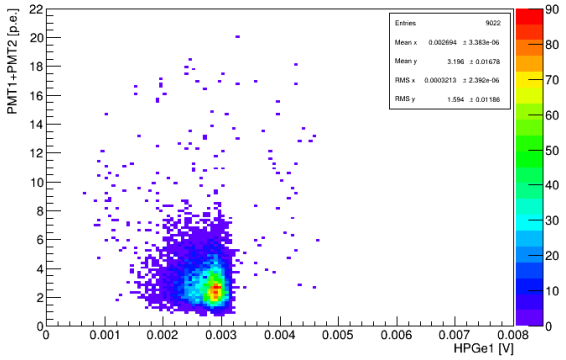

Figure 8. PMT sum vs HPGe1, calibration data cut for baseline, boundary, peaks, peak time and matched peaks.

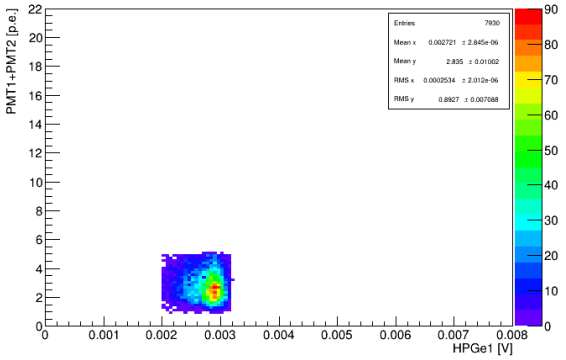

Figure 9. PMT sum vs HPGe1, calibration data cut for baseline, boundary, peaks, peak time, matched peaks and energy.

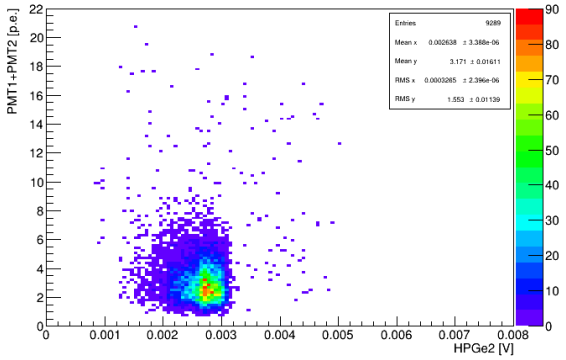

Figure 10. PMT sum vs HPGe2, calibration data cut for baseline, boundary, peaks, peak time and matched peaks.

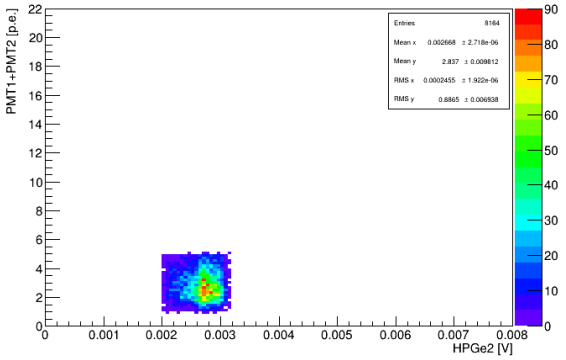

Figure 11. PMT sum vs HPGe2, calibration data cut for baseline, boundary, peaks, peak time, matched peaks and energy.

applied. The sum of the remaining events for both HPGe detectors after these cuts gives the net number used to determine the absolute efficiency calibration factor.

In order to verify the chance coincidence rate, the coincidence time windows were purposely shifted away from the actual coincidence peaks (offset matching cut).

4.3 Results

4.3.1 β/γ Coincidence Detection Efficiency

Table 8 summarises the results of the calibration run, giving the efficiencies for each data cut and the resulting count rates.

The acquired HPGe spectra are shown in Figure 12 and 13 for three different cuts. In both detectors, the 46.5 keV peak shows a low energy tail resulting in an increased resolution. These spectra are not background corrected because the background count rate is two orders of magnitudes smaller, and as such the background correction was considered as not essential. The combined gross count rate of both detectors, with the HPGe cuts applied and corrected for dead time, gives a value of 8.06 cps. Given the source activity of 518 Bq and the emission probability of 4.25%, an

Table 8. Summary of the analysis results for the calibration runs using a ^{210}Pb source. Given are applied data cuts for the specified channel combinations, the resulting event number, its fraction to the total event number and the dead time corrected rate. The uncertainties are given at 1σ and include statistical and systematic components.

Channel	Cuts	Events	Rate [cps]	Fraction
	Real time: 14748 s, True events:	149936	1.02E+01	
	Recorded events (valid waveforms):	80068	5.43E+00	
Ge1	peaks	35801	4.55E+00	44.7%
Ge1	peaks & baseline & ptime & energy	30059	3.82E+00	37.5%
Ge2	peaks	39192	4.98E+00	48.9%
Ge2	peaks & baseline & ptime & energy	30415	3.86E+00	38.0%
PMT1	peaks	39971	5.08E+00	49.9%
PMT1	peaks & boundary & baseline	31649	4.02E+00	39.5%
PMT2	peaks	40881	5.19E+00	51.1%
PMT2	peaks & boundary & baseline	32285	4.10E+00	40.3%
PMT1 & PMT2	peaks & bndry & bline & matched$_{PMT}$	20129	2.56E+00	25.1%
PMT1 & PMT2	" & energy	17940	2.28E+00	22.4%
PMT1 & PMT2	peaks & bndry & bline & offset$_{PMT}$	40	5.08E-03	0.0%
Ge1 & PMT1 & PMT2	basic & ptime & matched$_{PMTGe}$	9022	1.15E+00	11.3%
Ge2 & PMT1 & PMT2	basic & ptime & matched$_{PMTGe}$	9289	1.18E+00	11.6%
Ge1 & PMT1 & PMT2	" & energy	7930	1.01E+00	9.9%
Ge2 & PMT1 & PMT2	" & energy	8164	1.04E+00	10.2%
	Sum Ge1 + Ge2	16094	2.04E+00	20.1%
	Absolute efficiency, based on 518 Bq ^{210}Pb		**0.395±0.016 %**	
Ge1 & PMT1 & PMT2	basic & peaks & bline & offset$_{PMTGe}$	4	5.08E-04	0.0%
Ge2 & PMT1 & PMT2	basic & peaks & bline & offset$_{PMTGe}$	3	3.81E-04	0.0%
Ge1 & PMT1 & PMT2	" & energy	2	2.54E-04	0.0%
Ge2 & PMT1 & PMT2	" & energy	0	0.00E+00	0.0%
	Sum Ge1 + Ge2	2	2.54E-04	0.0%
	^{210}Pb equivalent activity, measured [Bq]		0.064±0.043	

absolute gamma efficiency of 36.6±0.4% at 46.5 keV was calculated. This compares reasonably well with the simulated value of 39.7% for the extended energy window between 30 and 50 keV.

After all cuts, including the coincidence requirement for PMTs and HPGe, and the energy window, the dead time corrected count rate is 2.04±0.05 cps for 518 Bq of ^{210}Pb. The resulting absolute efficiency was calculated to be 0.395±0.016%. This value is higher than the estimated 0.3% in Section **??**, but comparable given the assumptions made in the estimate.

4.3.2 Chance Coincidence Rate

To estimate the chance coincidence rate of this counting method, the PMT coincidence window and the PMT-HPGe coincidence window were shifted out of time. The PMT window was moved

from |Δt| = [0ns,40ns] to [460ns,500ns]. Only 40 out of 80068 events were retained after this cut. The count rate dropped by a factor of 500 compared to the coincidence setting, down to $5{\cdot}10^{-3}$ cps. This gives an indication that the random thermo-ionic noise emission spectrum is practically eliminated from the calibration source spectrum by the coincidence logic. The PMT-HPGe window was moved from [-250ns,0ns] to [250ns,500ns]. The sum of both HPGe detectors dropped down to 7 events, which corresponds to a reduction by a factor 2000 compared to the coincidence setting. The combined count rate is approximately $0.9{\cdot}10^{-3}$ cps. Applying the energy cut further reduces the number of events by a factor of 3. A PMT coincidence rate with the calibration source was known from previous tests to be 2227 cps. This rate however included some railing or noise signals. The combined singles rate from both HPGe detectors was 8.7 cps. With a window setting of 250 ns, the expected chance coincidence rate was calculated according Equation 2.1 to be $4.8{\cdot}10^{-3}$ cps, which is somewhat higher than the measured $0.9{\cdot}10^{-3}$ cps.

4.3.3 ^{210}Pb Detection Limit

The $^{Pb}210$ detection limit of the β/γ coincidence method was measured by counting the prepared background sample (a blank scintillator vial) inside the shielded sample holder, and applying the cuts determined from the ^{210}Pb calibration sample data analysis.

For this measurement 66 background runs were performed over a period of 26 days recording 675,064 waveforms. After a first exclusion of unusable runs based on the average trigger rates and a second cut after some data inspection, the number of runs was reduced to 32, giving a real measurement time of 9.2 days and live time of 5.9 days.

Unusable runs were generally identified by variations in the logged temperatures over the acquisition period, or by large increases in the trigger rate. One planned power outage on the 10th April required the whole setup to be shut down and re-powered, and on several occasions there were issues with the laboratory air conditioning system and the internal cooling system. The regular filling of LN_2, twice a week, could as well affect the system stability temporarily. The trigger setup was quite sensitive to noise induced on the HPGe signals. On several occasions, noise, most likely induced over the power supply network, increased trigger rates substantially. The external air cooler was observed to occasionally increase the trigger rates, however this increase was not always observed. No final conclusion could be drawn on the origin of the noise appearing from time-to-time and increasing the trigger rate by factors of 200 or more. A total of 11 runs were identified to differ by more than 20% from the average trigger rate and were excluded from the analysis as this implied changing S/N ratios and the impossibility to correct for the non-constant system dead time. This data cut is referred to as run cut 1 in the last column of Table **??**. kVariation in the laboratory environmental conditions also produced observable drift in the baselines, these runs were excluded by run cut 2 in Table **??**. In the cleaned data set, excluding the unusable runs described above, the rms of the baseline histograms from the cleaned background data set are comparable to those of the calibration run. The amplitudes and peak times for all channels as well as the time differences between PMT and HPGe peaks against the trigger time did not show any important features with respect to the trigger time.

The cuts defined on the calibration data to identify the ^{210}Pb β-γ signal coincidence were applied to the background data set. This data set shows the same timing features as the calibration data set: the resultant peak in the histogram of all PMT-HPGe channel combinations is a clear

signature for time correlated events, and the peak position corresponds exactly to the coincidence peak position in the calibration data set, extending from -250 ns to 0 ns.

The pulse height spectra of coincident PMT peaks in the background data set after all cuts are shown together with the calibration source sum spectrum in Figure 15. The background spectrum showed a greater mean value of 4.5 p.e. compared to 3.1 p.e. for the calibration source. This difference indicates that a higher energy beta/electron radiation component is contributing to the background while fulfilling all the coincidence criteria. The PMT average peak widths are larger than found in the in the calibration, which matches with the observation of higher average peak amplitudes in the background data set.

The HPGe pulse height spectra for both detectors are shown in Figures 16 to 19. Figures 16 and 18 show the linear scale spectra for HPGe 1 and 2, only cut for the presence of peaks. On both histograms, a background was fitted, which was subsequently subtracted to analyse the remaining peaks. The peak positions were determined for the three main peaks (excluding the first visible peak, which is due to noise or low energy X rays). The peak at 2.9 mV corresponds to the 46.5 keV emission from ^{210}Pb. The two other peaks at 4.0 mV ($\equiv$62.6 keV) and 5.9 mV ($\equiv$90.7 keV) are attributed to the ^{234}Th gamma emissions at 63.3 keV and 92.6 keV. The gross count rates in the region of interest were determined for the 46.5 keV peak (Table 9).

Table 9. Integral and background net count rate for the 46.5 keV peak at a live time of 510'860 seconds.

Detector	Lower limit [keV]	Upper limit [keV]	Gross Σ [cts]	Net Σ [cts]	Gross rate [$s^{-1}keV^{-1}$]	Gross rate (Table 3) [$s^{-1}keV^{-1}$]
HPGe1	38.7	50.6	21661	5566	0.0036	0.0025
HPGe2	40.5	51.1	24445	8730	0.0045	0.0050

Figures 17 and 19 show the same spectra in logarithmic scale with overlaid pulse height distributions where data quality cuts were applied. The blue curves result after the application of basic and coincidence conditions cuts. The red spectra have in addition cuts applied for peak time and the restricted energy window between 1 and 5 p.e. for the PMT sum. The clear ^{210}Pb and ^{234}Th peaks have disappeared after the coincidence conditions cuts. One can conclude that this major background was therefore external to the source volume. Another observation is that the high energy part above 4.5 mV is mainly removed by cutting misplaced triggered events from the data set. The reason for this, as the reason for the misplaced triggered events, could not be elucidated.

The fully cut spectra were again plotted separately on a linear scale in Figures 20 and 21. In addition to a broad plateau, two peaks can be seen at 3.3 mV and 4 mV, more clearly on detector 1 than detector 2. No plausible emitter could be identified for 3.3 mV ($\equiv$51.8 keV). The peak at 4 mV ($\equiv$62.6 keV) most likely corresponds to ^{234}Th, which is a beta emitter at relatively low energy (105 keV endpoint). This decay branch is accompanied by a coincident gamma at 63.3 keV (I_γ=3.75%) within less than 1 ns [41, 42]. On the other hand, the same beta decay can be followed by a equally fast 92.6 keV (I_γ=4.3%) emission, which is not at all visible in the spectrum.

The 2D histograms of the summed PMT vs. each HPGe are given in Figures 22 to 25, once with and without the energy cut. The plots do not reveal additional information, showing a featureless histogram with the main events in the region between 1 and 4.5 mV and from 1 to 8 p.e..

Table 10 lists the results of the different cuts applied on the background measurement data with their respective survival fraction and dead time corrected count rate. After the final cut, the remaining event rate was used to calculate an activity value based on the efficiency determined from the ^{210}Pb calibration. The retained ^{210}Pb-equivalent activity of 356$\pm$35 mBq is much higher than expected from the estimate in Section 3.1 for the chance coincidence background. Considering a similar measurement time and uncertainty for a actual sample, the detection limit at 2σ will amount to 140 mBq.

A likely explanation could be the contamination of the sample with naturally occurring radioactivity. ^{210}Pb is ubiquitous as a descendent of Radon. It is possible that the utensils used for the sample preparation such as the pipettes or the vial itself had been exposed to Radon and contaminated beforehand. Although the equipment had been rinsed before use with ultra-pure water, a remaining substantial level of activity cannot be excluded. Another potential contamination through the scintillation cocktail itself might be considered. It seems though rather improbable as these agents are used for low level ^{3}H detection and an activity of O(300mBq) in 15 ml might have been detected already in a commercial low level detector.

The gamma spectrum analysis done in the previous chapter gives an indication that the found contamination might not be due at all or solely to ^{210}Pb, lacking a clearly identified peak. ^{234}Th is a candidate for being present in the sample, considering the peak identification at 62.8 keV and that

Table 10. Summary of the analysis results for the background runs using a blank sample of HNO_3. Given are applied data cuts for the specified channel combinations, the resulting event number, its fraction to the total event number and the dead time corrected rate. The uncertainties are given at 1σ and include statistical and systematic components.

Channel	Cuts	Events	Rate [cps]	Fraction
	Real time: 793253 s, True events:	496181	6.26E-01	
	Recorded events (valid waveforms):	319525	4.03E-01	
Ge1	peaks	97393	1.91E-01	30.5%
Ge1	peaks & baseline & ptime & energy	25423	4.98E-02	8.0%
Ge2	peaks	116735	2.29E-01	36.5%
Ge1	peaks & baseline & ptime & energy	30965	6.06E-02	9.7%
PMT1	peaks	14390	2.82E-02	4.5%
PMT1	peaks & boundary & baseline	13772	2.70E-02	4.3%
PMT2	peaks	13980	2.74E-02	4.4%
PMT2	peaks & boundary & baseline	13139	2.57E-02	4.1%
PMT1 & PMT2	peaks & bndry & bline & matched$_{PMT}$	5276	1.03E-02	1.7%
PMT1 & PMT2	" & energy	3344	6.55E-03	1.0%
PMT1 & PMT2	peaks & bndry & baseline & offset	7	1.37E-05	0.0%
Ge1 & PMT1 & PMT2	basic & ptime & matched$_{PMTGe}$	1496	2.93E-03	0.5%
Ge2 & PMT1 & PMT2	basic & ptime & matched$_{PMTGe}$	1786	3.50E-03	0.6%
Ge1 & PMT1 & PMT2	" & energy	336	6.58E-04	0.1%
Ge2 & PMT1 & PMT2	" & energy	381	7.46E-04	0.1%
	Sum Ge1 + Ge2	717	1.40E-03	0.2%
	^{210}Pb equivalent activity, measured [Bq]		**0.356±0.035**	
Ge1 & PMT1 & PMT2	basic & ptime & offset$_{PMTGe}$	0	0.00E+00	0.0%
Ge2 & PMT1 & PMT2	basic & ptime & offset$_{PMTGe}$	0	0.00E+00	0.0%
Ge1 & PMT1 & PMT2	" & energy	0	0.00E+00	0.0%
Ge2 & PMT1 & PMT2	" & energy	0	0.00E+00	0.0%
	Sum Ge1 + Ge2	0	0.00E+00	0.0%
	^{210}Pb equivalent activity, measured [Bq]		<4.96E-04	

this isotope can also generate coincident events in both detectors. A better gamma energy resolution could identify and reject this isotope, while its Compton background would certainly affect the energy region of interest. A doubt remains, as the 92.6 keV peak of ^{234}Th is clearly absent from the final spectrum. Another peak apparently forming at 51.8 keV could not be assigned to any plausible radionuclide. The origin of the remnant counting plateau seen in the reduced gamma spectrum also could not be determined. A possible explanation could be the detection of Compton scattered photons by the liquid scintillator and their subsequent detection in the HPGe detectors. Such an effect could explain a featureless spectrum. No attempt was made to estimate the probability of such a process at the given external background radiation levels lacking a complete simulation model incorporating both gamma and beta detectors.

Table 11. Relative uncertainty values determined for different data cuts from varying the cut parameters on the calibration and background data set.

Uncertainty	Variation	Type	Distribution	Divisor	Relative uncertainty	
					Calibration	Background
Matched$_{PMT}$ cut	$\pm$ 4 ns	B	Rectangular	$\sqrt{3}$	0.8%	0.6%
Matched$_{PMT-HPGe}$ cut	$\pm$ 4 ns	B	Rectangular	$\sqrt{3}$	0.5%	0.4%
Peak time cut	$\pm$ 10 ns	B	Rectangular	$\sqrt{3}$	0.1%	1.3%
Energy cut PMT sum	$\pm$ 0.1 p.e.	B	Rectangular	$\sqrt{3}$	1.2%	1.5%
Energy cut HPGe	$\pm$ 0.1 mV	B	Rectangular	$\sqrt{3}$	2.8%	4.0%
^{210}Pb Source activity		B	Rectangular x 2	$\sqrt{12}$	1.1%	
Counting uncertainty		A	Normal	1	0.8%	3.7%
Calibration factor		B	Rectangular x 2	$\sqrt{12}$	**4.1%**	4.1%
Background activity						**9.4%**

The uncertainties of the calibration factor and the ^{210}Pb-equivalent background activity were calculated from the statistical counting uncertainties, the calibration source uncertainty and systematic uncertainties. The latter were determined experimentally by varying the cut parameters for the coincidence time matching, peak time and energy cuts. The variations were chosen arbitrarily from assumed potential value shifts during operation. Table 11 lists the contributions to the relative uncertainties of the calibration factor and the determined background activity.

The ultimate performance of the coincidence method, in the absence of background in the sample matrix, can be estimated from the chance coincidence rate. As for the calibration data set, the chance coincidence rate was checked by shifting the coincidence windows away from the coincidence peak. The window settings were the same as for the calibration data. As expected, the events surviving all cuts and the offset cut, dropped to very low numbers (see Table 10), and no events finally passed the energy cut. Considering the effective live time and efficiency calibration factor, a maximum activity value of 0.496 mBq was calculated, corresponding to one count whilst the detector was live. Not considering a background contribution from the liquid scintillator and sample, this would represent the lowest detection limit of the system for the given measurement time.

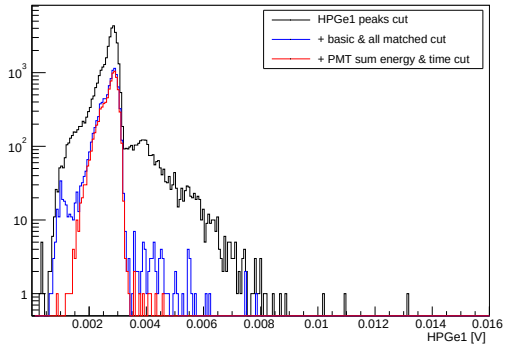

Figure 12. Calibration pulse height spectra of HPGe1 with different data cuts; the blue spectrum was cut for baseline, boundary, peak, matchedPMT and matchedPMT-HPGe. The red spectrum additionally was cut for PMT sum energy and peak time.

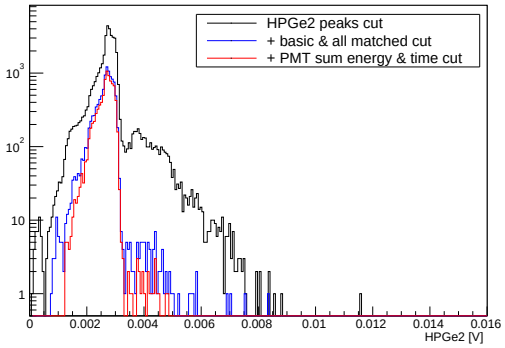

Figure 13. Calibration pulse height spectra of HPGe2 with different data cuts; the blue spectrum was cut for baseline, boundary, peak, matchedPMT and matchedPMT-HPGe. The red spectrum additionally was cut for PMT sum energy and peak time.

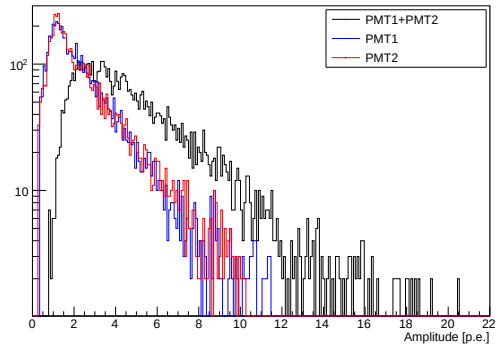

Figure 14. PMT single and sum spectra for coincident PMT peaks. The mean value of the sum spectrum is 4.5±2.7 p.e..

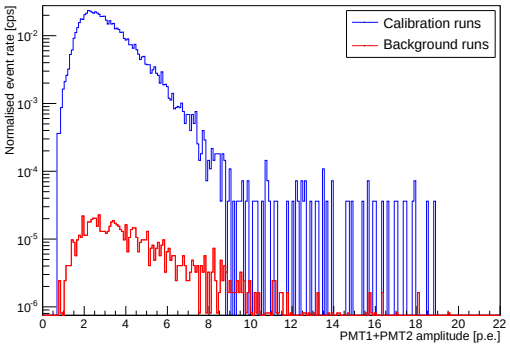

Figure 15. PMT sum spectra from the calibration and background runs, normalised and dead time corrected. The mean values are 3.1±1.4 p.e. and 4.5±2.7 p.e. for the calibration and background spectrum, respectively.

5. Conclusions

In this work the concept of a beta/gamma coincidence measurement system to detect low levels of ^{210}Pb was developed. After initial estimates and simulations to check for its feasibility and expected performance, the detector system was designed, assembled, tested and finally installed at the STFC Boulby Underground Laboratory. The data acquisition system including control and acquisition software was developed and adapted to operate the system at the remote underground location. Several data acquisition runs were made to set up and tune the system. Finally, a calibration and a longterm background measurement were performed and analysed.

The absolute detection efficiency of 0.395±0.016%, as determined in the calibration measurement for ^{210}Pb, was close to the initially estimated expected value of 0.3%. As such, the results proved the systems functionality and correct choice of parameter settings to detect ^{210}Pb

beta/gamma coincident events.

The first attempt to reach the low detection limit objective was not successful. A coincidence count rate of a factor 400 to 1000 above the required level was found with the prepared background sample. The ^{210}Pb -equivalent background activity of 356±35 mBq would lead to a detection limit of 140 mBq for a live time of 5.9 days, about a factor 140 higher than the typical limits achieved in the best alpha spectrometric method to quantify ^{210}Pb. Regarding the long measurement time and comparatively complex data analysis process, the method offers no advantage at the moment over the standard measurement methods.

However, the coincidence concept in itself is not the cause the high background level, and so there is still unlocked potential for this technique. It is suspected that real background events are accountable for this result. The most likely explanation for the background is a contamination of the sample during the preparation process. Secondly, an intrinsic contamination of the used agents could be the cause. Thirdly, the effect of external radiation producing Compton scattered electrons in the scintillator while detecting the scattered photon in the HPGe detectors might be considered. There is room for substantial improvement in the sample handling, as no special care was taken to use radio-pure materials, and much lower background HPGe detectors are readily available. Shorter time coincidence windows could be achieved, in principle by as much as a factor of 5-10, by using a scintillator optimised for fast counting.

The ultimate performance of the coincidence method, in the absence of background in the sample matrix, can be estimated from the chance coincidence rate. As in the calibration data set, the chance coincidence rate was checked by shifting the coincidence windows away from the coincidence peak in the background data set. The window settings were the same as for the calibration data. As expected, the events surviving all cuts and the offset cut, dropped to very low numbers (see Table 10), and no events finally passed the energy cut. Considering the effective live time and efficiency calibration factor, a maximum activity value of 0.496 mBq was calculated, corresponding to one count whilst the detector was live. Not considering a background contribution from the liquid scintillator and sample, this would represent the lowest detection limit of the system for the given measurement time.

Acknowledgments

Acknowledgments.

References

[1] A. Zaborska, J. Carroll, C. Papucci, and J. Pempkowiak, *Intercomparison of alpha and gamma spectrometry techniques used in 210Pb geochronology*, *Journal of Environmental Radioactivity,* **93***, no. 1, pp. 38–50, 2007.*, .

[2] A. Martin and S. A. Harbison, *An Introduction to Radiation Protection*, 5th ed., Oxford University Press,USA, Sep. 2006.

[3] M. Boulay, *Radon diffusion and acrylic background requirements for DEAP-3600*, Tech. Rep. DEAP STR-2009-006, Nov. 2009.

[4] NNDC, *Evaluated and compiled nuclear structure data: ENSDF dataset retrieval*, 2013.

[5] E. Browne, "Nuclear data sheets for a = 210," *Nuclear Data Sheets*, vol. 99, no. 3, pp. 649–752, Jul. 2003.

[6] X. Hou and P. Roos, "Critical comparison of radiometric and mass spectrometric methods for the determination of radionuclides in environmental, biological and nuclear waste samples," *Analytica Chimica Acta*, vol. 608, no. 2, pp. 105–139, Feb. 2008.

[7] S. J. Goldstein and C. H. Stirling, *Techniques for measuring uranium-series nuclides: 1992–2002*," *Reviews in Mineralogy and Geochemistry*, vol. 52, no. 1, pp. 23–57, Jan. 2003. [Online]. Available:

[8] Y. Y. Ebaid and A. E. M. Khater, *Determination of 210Pb in environmental samples*," *Journal of Radioanalytical and Nuclear Chemistry*, vol. 270, no. 3, pp. 609–619, Dec. 2006. [Online]. Available:

[9] A. Nachab and P. Hubert, "210Pb activity by detection of bremsstrahlung in 210Bi β-decay," *Nuclear Instruments and Methods in Physics Research Section B: Beam Interactions with Materials and Atoms*, vol. 274, no. 0, pp. 188–190, Mar. 2012. [Online]. Available:

[10] F. Henricsson, Y. Ranebo, E. Holm, and P. Roos, "Aspects on the analysis of 210Po," *Journal of Environmental Radioactivity*, vol. 102, no. 5, pp. 415–419, May 2011. [Online]. Available:

[11] KIT, "Analytische labore - nachweisgrenzen," http://www.ksm.kit.edu/196.php, 2013. [Online]. Available:

[12] L. Laureano-Pérez, R. Collé, R. Fitzgerald, I. Outola, and L. Pibida, "A liquid-scintillation-based primary standardization of 210Pb," *Applied Radiation and Isotopes*, vol. 65, no. 12, pp. 1368–1380, Dec. 2007. [Online]. Available:

[13] D. Woods, N. Bowles, S. Jerome, P. de Lavison, S. Lineham, J. Makepeace, A. Woodman, and M. Woods, "Standardisation of 210Pb," *Applied Radiation and Isotopes*, vol. 52, no. 3, pp. 381–385, Mar. 2000. [Online]. Available:

[14] R. Fitzgerald and M. Schultz, "Liquid-scintillation-based anticoincidence counting of co-60 and pb-210," *Applied Radiation and Isotopes*, vol. 66, no. 6–7, pp. 937–940, Jun. 2008. [Online]. Available:

[15] A. Baerg, "Multiple channel 4pi.beta-gamma anti-coincidence counting," *Nuclear Instruments and Methods in Physics Research*, vol. 190, no. 2, pp. 345–349, Dec. 1981. [Online]. Available:

[16] G. F. Knoll, *Radiation Detection and Measurement*, 4th ed. Wiley, Aug. 2010.

[17] PerkinElmer, "Liquid scintillation cocktails - tech support - PerkinElmer reagents technical support wiki," http://www.perkinelmer.com/Resources/TechnicalResources/ApplicationSupportKnowledgebase/radiometric/scint_cocktai 2012.

[18] CANBERRA Industries Inc., "Reverse electrode coaxial ge detectors (REGe) data sheet," 2010. [Online]. Available:

[19] A. Murphy and S. Paling, "The boulby mine underground science facility: The search for dark matter, and beyond," *Nuclear Physics News*, vol. 22, no. 1, pp. 19–24, 2012. [Online]. Available:

[20] M. Robinson, V. Kudryavtsev, R. Lüscher, J. McMillan, P. Lightfoot, N. Spooner, N. Smith, and I. Liubarsky, "Measurements of muon flux at 1070 m vertical depth in the boulby underground laboratory," *Nuclear Instruments and Methods in Physics Research Section A: Accelerators, Spectrometers, Detectors and Associated Equipment*, vol. 511, no. 3, pp. 347–353, Oct. 2003. [Online]. Available:

[21] J. Hubbell and S. Seltzer, "NIST: x-ray mass attenuation coefficients," http://www.nist.gov/pml/data/xraycoef/index.cfm, May 1996. [Online]. Available:

[22] PerkinElmer, "Material safety data sheet - ultima gold LLT," Feb. 2009.

[23] PerkinElmer, "ULTIMA gold uLLT - for ultra low level counting," 2008.

[24] J. Elisabeth Wieslander, M. Hult, J. Gasparro, G. Marissens, M. Misiaszek, and W. Preusse, "The sandwich spectrometer for ultra low-level γ-ray spectrometry," *Applied Radiation and Isotopes*, vol. 67, no. 5, pp. 731–735, May 2009. [Online]. Available:

[25] D. Sanderson, "Private communication," 2012.

[26] PerkinElmer, "Scintillation cocktails & consumables," 2007.

[27] The plasticshop.co.uk, "Mechanical properties data sheet for acrylic rod," 2013. [Online]. Available:

[28] F. Verrezen, H. Loots, and C. Hurtgen, "A performance comparison of nine selected liquid scintillation cocktails," SCK CEN, Mol, Belgium, Tech. Rep. SCK•CEN-BLG-1052, Jun. 2008. [Online]. Available:

[29] L. Pujol and J. Sanchez-Cabeza, "Optimisation of liquid scintillation counting conditions for rapid tritium determination in aqueous samples," *Journal of Radioanalytical and Nuclear Chemistry*, vol. 242, no. 2, pp. 391–398, 1999. [Online]. Available:

[30] J. ter Wiel and T. Hegge, "Advances in scintillation cocktails," Gatlinburg, Tennessee, Oct. 1989. [Online]. Available:

[31] N. Pérron and P. Cassette, "Absolute efficiency of LS cocktails using a compton coincidence method," 1994. [Online]. Available:

[32] D. Akimov, H. Araújo, E. Barnes, V. Belov, A. Burenkov, V. Chepel, A. Currie, B. Edwards, V. Francis, C. Ghag, A. Hollingsworth, M. Horn, G. Kalmus, A. Kobyakin, A. Kovalenko, V. Lebedenko, A. Lindote, M. Lopes, R. Lüscher, K. Lyons, P. Majewski, A. Murphy, F. Neves, S. Paling, J. Pinto da Cunha, R. Preece, J. Quenby, L. Reichhart, P. Scovell, V. Solovov, N. Smith, P. Smith, V. Stekhanov, T. Sumner, R. Taylor, C. Thorne, and R. Walker, "The ZEPLIN-III anti-coincidence veto detector," *Astroparticle Physics*, vol. 34, no. 3, pp. 151–163, Oct. 2010. [Online]. Available:

[33] ET Entreprises, "PMT 9302B series data sheet," Sep. 2010. [Online]. Available:

[34] C. Ghag, "Private communication," 2013.

[35] G. Milton, S. Kramer, R. Deal, and E. Earle, "Ultra trace analysis of acrylic for 232Th and 238U daughters," *Applied Radiation and Isotopes*, vol. 45, no. 5, pp. 539–547, May 1994. [Online]. Available:

[36] B. Cleveland, "Acrylic assay," Tech. Rep., Mar. 2009. [Online]. Available:

[37] C. Nantais, "Measurement of the radiopurity of acrylic for the DEAP-3600 dark matter experiment," Perimeter Institute, Jul. 2011. [Online]. Available:

[38] G. Choppin, J. Rydberg, and J.-O. Liljenzin, *Radiochemistry and Nuclear Chemistry, Third Edition*, 3rd ed. Butterworth-Heinemann, Nov. 2001.

[39] R. Brun and F. Rademakers, "ROOT — an object oriented data analysis framework," *Nuclear Instruments and Methods in Physics Research Section A: Accelerators, Spectrometers, Detectors and Associated Equipment*, vol. 389, no. 1–2, pp. 81–86, Apr. 1997. [Online]. Available:

[40] J. Monroe and S. Henderson, "Neutron veto - waveform processing library for ROOT," Aug. 2012.

[41] A. Luca, "234Th - comments on evaluation of decay data," Jun. 2009. [Online]. Available:

[42] E. Browne and J. Tuli, "Nuclear data sheets for a = 234," *Nuclear Data Sheets*, vol. 108, no. 3, pp. 681–772, Mar. 2007. [Online]. Available:

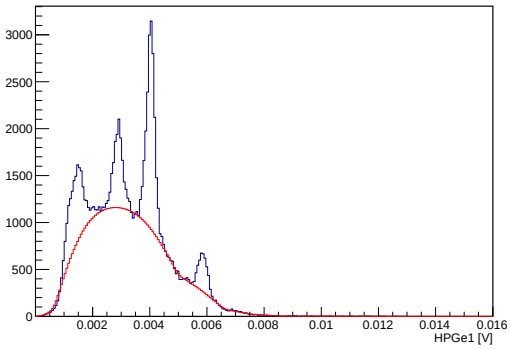

Figure 16. Background pulse height spectrum of HPGe1 including a fitted background estimator (red line); data cut for peaks.

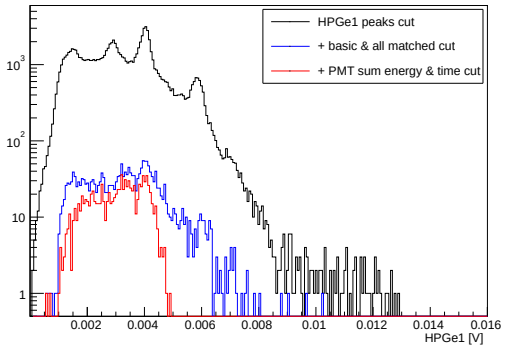

Figure 17. Background pulse height spectra of HPGe1 with different data cuts; the blue spectrum was cut for baseline, boundary, peak, matched$_{PMT}$ and matched$_{PMT-HPGe}$. The red spectrum additionally was cut for PMT sum energy and peak time.

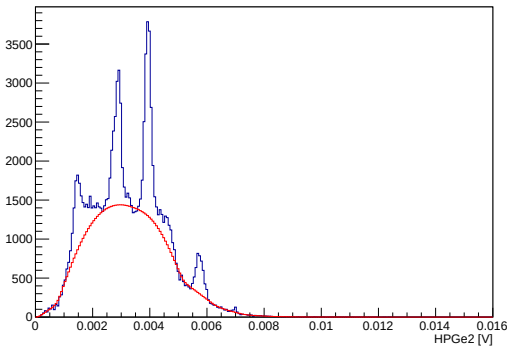

Figure 18. Background pulse height spectrum of HPGe2 including a fitted background estimator (red line); data cut for peaks.

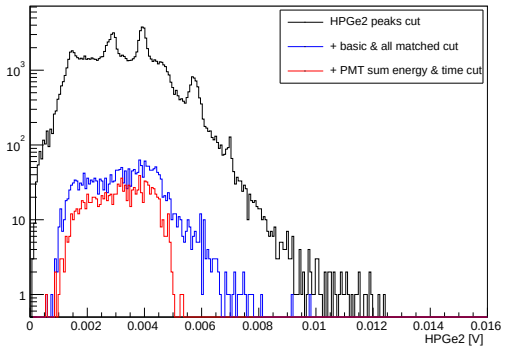

Figure 19. Background pulse height spectra of HPGe2 with different data cuts; the blue spectrum was cut for baseline, boundary, peak, matched$_{PMT}$ and matched$_{PMT-HPGe}$. The red spectrum additionally was cut for PMT sum energy and peak time.

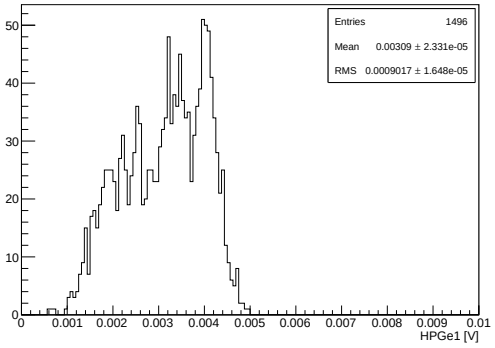

Figure 20. Background pulse height spectra of HPGe1 on linear scale, full data cut for peaks, baseline, boundary, matched peaks, peak time and PMT sum energy.

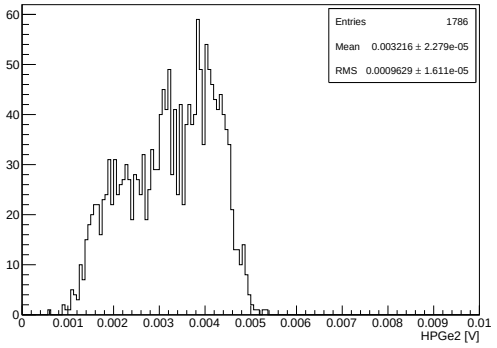

Figure 21. Background pulse height spectra of HPGe2 on linear scale, full data cut for peaks, baseline, boundary, matched peaks, peak time and PMT sum energy.

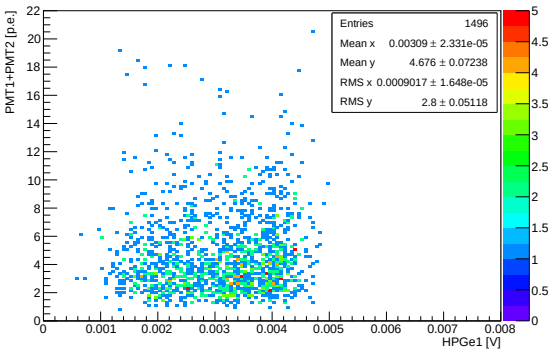

Figure 22. Sum of PMT amplitudes vs. HPGe1 amplitudes; basic cut, peak time cut and matched peaks cut applied on the background data.

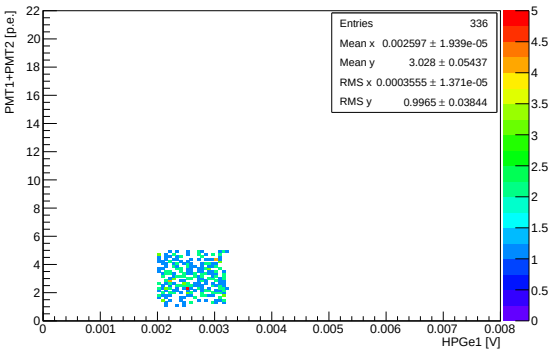

Figure 23. Sum of PMT amplitudes vs. HPGe1 amplitudes; basic cut, peak time cut, matched peaks and energy cuts applied on the background data.

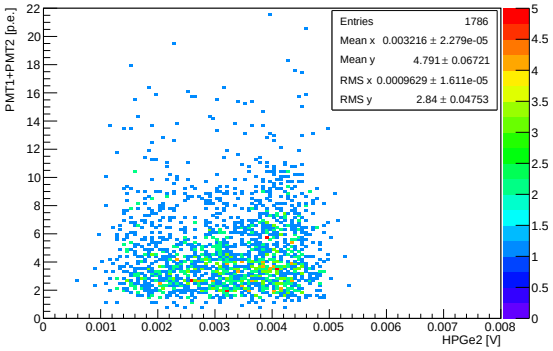

Figure 24. Sum of PMT amplitudes vs. HPGe2 amplitudes; basic cut, peak time cut and matched peaks cut applied on the background data.

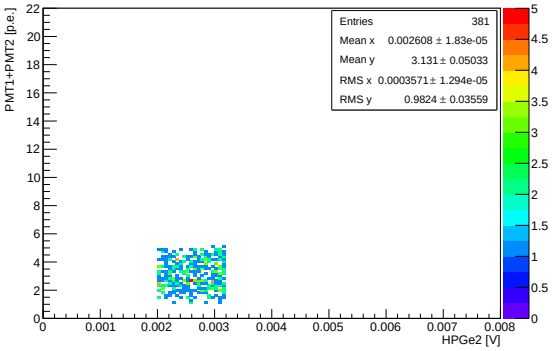

Figure 25. Sum of PMT amplitudes vs. HPGe2 amplitudes; basic cut, peak time cut, matched peaks and energy cuts applied on the background data.